Propylammonium Nitrate as a Solvent for Amphiphile Self-Assembly into Micelles, Lyotropic Liquid Crystals, and Microemulsions

Rob Atkin,*,† Sophie M. C. Bobillier,‡ and Gregory G. Warr‡

School of Environmental and Life Sciences, The University of Newcastle, Callaghan, NSW 2308, Australia, and School of Chemistry, F11, The University of Sydney, NSW 2006, Australia

Received: November 8, 2009; Revised Manuscript Received: December 1, 2009

The phase behavior and self-assembled microstructures of a range of oligo(oxyethylene)-*n*-alkyl ether (C_iE_j) surfactants has been investigated in propylammonium nitrate (PAN), a room temperature ionic liquid. Micelles and single-phase microemulsions were all found to form at alkyl chain lengths from dodecyl to octadecyl, and lyotropic liquid crystals formed with hexadecyl chains or longer. Small-angle neutron scattering (SANS) shows that self-assembly occurs by solvophobic interactions driving the aggregation of the alkyl chains, but several results indicate that these are weaker in PAN than in water or ethylammonium nitrate, due chiefly to the hydrophobicity of PAN. Longer alkyl chains are needed for lyotropic liquid crystals to form, and higher surfactant concentrations are needed to form a single phase microemulsion. Conductivity shows these microemulsions to be weakly structured, and relatively insensitive to oil or surfactant molecular structure, unlike water-based systems. However, SANS contrast variation reveals a nanosegregation of oil from the alkyl tails of surfactants within the microemulsion, and may suggest a cosurfactant-like role for the propylammonium cation. Molecular areas within microemulsions and lamellar phases are larger than corresponding water- or ethylammonium nitrate-based systems due to the large molecular volume of the solvating PANs.

Introduction

Room temperature ionic liquids (ILs) are currently attracting a great deal of research interest.[1,2] They usually consist of a bulky organic cation and a weakly interacting anion. Compared to a typical inorganic salt, the ionic charge is distributed over large molecular volumes by resonance, decreasing Coloumbic attractions, while steric interactions hinder the ability of the ions to pack tightly into a crystal lattice. The combination of these two effects produces low melting points. ILs have increasingly been employed as solvents for chemical synthesis and catalysis due to their (often) negligible vapor pressure, wide temperature stability range, and "designer properties", which refers to the ability to tune physical properties by modifying molecular structure.[1,3] ILs often have high conductivity and redox stability, so they are frequently employed as electrolytes.

While the oldest known ILs are protic primary ammonium salts,[4−8] many ILs contain a quaternary organic nitrogen (e.g., quaternary ammonium[9,10] and alkylpyridinium[11]) or phosphorus cation coupled to a range of anions. The 1-alkyl-3-methylimidazolium salts are the focus of intense research interest because changing the length or species of the alkyl moiety allows melting point and solvent characteristics to be controlled. The anion species also influences physical properties, and an increasingly wide variety of ions is available, ranging form nitrate or chloride to more complex structures such as tetrafluoroborate, hexafluorophosphate, methylsulfate, and trifluoromethylsulfate. Depending on structure, ILs may be miscible with oil or water, i.e., hydrophilic or hydrophobic. To date, physical studies of ILs have largely focused on conductivity,[12] viscosity,[13] dissolution of small molecules,[14] solvation layers,[15,16] and the bulk structural organization of the IL.[17−19]

Surfactant aggregation in ILs has the potential to greatly increase utility via, for example, the formation of nanostructured reaction media or the ability to control interfacial properties. Several recent articles have reported micellization in pure IL solvents.[4,20−28] Our group has reported other important forms of surfactant self-assembly using alkyl oligoethyleneoxide (C_iE_j) surfactants in ethylammonium nitrate (EAN), which forms an extended hydrogen bonding network similar to water,[29] including adsorbed surfactant aggregates on graphite,[30] liquid crystalline phases,[31] and structured microemulsions.[32] The experiments presented in this Article examine the effect of using propylammonium nitrate (PAN) in place of EAN on surfactant self-assembly in binary (micelles and liquid crystals) and ternary (microemulsions) systems.

Compared to EAN, PAN has a lower melting point and reduced conductivity and density but increased viscosity.[33] Recent SANS experiments with selectively deuterated EAN and PAN have conclusively shown that both of these ILs possess nanoscale heterogeneity in the bulk.[19] Nanostructuring is due to electrostatic attractions between the ammonium cation and nitrate anion, favoring the creation of ionic domains.[34] The attraction between these groups will be enhanced by hydrogen bonding.[4,5] This results in solvophobic interactions *within the IL itself* that promote clustering of alkyl groups into nonpolar domains. The SANS structure peak was substantially more pronounced for PAN compared to EAN, consistent with greater segregation and a stronger solvophobic effect due to the longer cation alkyl chain.

In two previous papers we examined nonionic surfactant self-assembly into micelles[21] and liquid crystals[31] in EAN. The key difference between EAN- and water-based systems is that longer surfactant alkyl chains are necessary to drive self-assembly in

* To whom correspondence should be addressed. E-mail: rob.atkin@newcastle.edu.au.
† The University of Newcastle.
‡ The University of Sydney.

10.1021/jp910649a
Published on Web 12/29/2009

EAN. At low concentrations, nonionic surfactants in EAN aggregate into conventionally structured micelles with a hydrocarbon core surrounded by a corona of ethoxy groups. While micelles formed by dodecyl-chained surfactants are weakly structured, when the alkyl chain length was increased to tetradecyl or longer, well-defined aggregates formed, very similar to aqueous micelles. The structural trends noted for increasing surfactant alkyl and ethoxy chain length, and temperature, were consistent with results for aqueous systems.[21] At higher concentrations, nonionic surfactants form liquid crystal mesophases in EAN remarkably similar to those formed in water.[31]

The phase behavior of ternary surfactant systems is significantly more complicated than that of binary systems. In the paragraphs below, the properties of aqueous microemulsions and the methods and terminology used for elucidating and describing thermodynamic properties are described. This is followed by a brief review of our recent paper detailing the effect of using EAN in place of water on microemulsion phase behavior and microstructure. This discussion provides context for analyzing the results described in this manuscript using PAN as the polar phase.

Traditional microemulsions are optically transparent mixtures of water (or brine) and oil stabilized by surfactants. The surfactant molecules form an interfacial film that segregates aqueous and hydrocarbon domains and imparts a spreading pressure that greatly reduces interfacial tension, resulting in thermodynamic stability. C_iE_j surfactants are frequently employed in the study of these systems, as solvation of the surfactant headgroup, and therefore the film curvature, is a function of temperature. This allows highly systematic studies to be completed.[35] At low temperatures, the headgroup is strongly hydrated and the surfactant film curves toward the oil phase, producing droplets of oil in water. At high temperatures, the headgroup is dehydrated and contracted, favoring production of water droplets in oil. At intermediate temperatures, the interfacial tension approaches zero, and a zero mean curvature bicontinuous (sponge) structure[36] may form in which the surfactant separates disordered aqueous and oil regions.

The phase behavior of microemulsions is typically investigated by "slicing" the phase prism at a 1:1 ratio of polar to nonpolar solvent while increasing the surfactant concentration. The number of phases present is then recorded as a function of temperature.[37−39] At low to intermediate surfactant concentrations, miscibility gaps in the surfactant−water, surfactant−oil. and oil−water systems can, at appropriate temperatures, produce three-phase mixtures. In such mixtures, the upper and lower phases are oil and water, respectively, and the middle phase is a surfactant rich microemulsion. Increasing the surfactant concentration leads to the volume of the middle phase increasing, and at sufficiently high concentrations, a single-phase mixture forms. The phase diagram that describes this behavior has become known as the Kahlweit "fish" on account of its shape.[32,35,37] Many microemulsion properties are defined by the size and position of the fish, characterized by three important parameters.[37] ΔT is the maximum temperature interval over which the three-phase body occurs. $\bar{T}$ is the mean temperature of the three-phase body, at which the ability of the surfactant to simultaneously dissolve oil and water is maximized. The position in the phase diagram where the fish body meets the fish tail is denoted $\bar{X}$, which is defined by $\bar{T}$ and the surfactant efficiency (the minimum surfactant concentration required to completely dissolve the oil and water phases). These features are shown diagrammatically elsewhere.[32] In aqueous systems, $\bar{T}$ is determined by the interplay between the lower consolute temperature (T_β) in the binary water−surfactant system (the cloud point) and the upper consolute temperature (T_α) in the binary oil−surfactant system.[32,37] T_α and T_β change in a predictable fashion with variation in the system parameters i (number of CH_2 units in the tailgroup), j (number of ethoxy units in the headgroup), and k (number of CH_2 units in the alkane solvent).

Our preceding study of C_iE_j−alkane−EAN microemulsions[32] showed these systems have many features in common with corresponding aqueous systems, the primary difference being that increased surfactant concentrations and longer tailgroups are required, in accordance with results for binary systems.[21,31] Variation in the length of the surfactant headgroup, tailgroup, and the alkane alter phase behavior in a manner consistent with aqueous microemulsions. The change in conductivity as a function of temperature showed that EAN microemulsions were strongly structured for surfactant chain lengths longer than 12, and small-angle X-ray scattering (SAXS) was used to probe morphology. SAXS spectra from the single-phase region consisted of a single broad scattering peak qualitatively similar to that observed in aqueous systems. However, fitted domain sizes were substantially lower than that reported for similar water-based microemulsions, and the ratio of the domain size to correlation length was markedly reduced, showing that the EAN and oil domains remain correlated over more internal interfaces. The overall picture for EAN microemulsions is one of high surfactant concentrations producing small, structured domains with highly correlated interfaces.

Materials and Methods

99% pure alkyl oligoethyleneoxide (C_iE_I) surfactants were obtained from BioChemika or Nikkol Chemical Company, and were used without further purification. Partially deuterated $C_{14}E_4$ and $C_{18}E_4$ (deuterated tailgroup, hydrogenous headgroup, henceforth referred to as d_{29}-$C_{14}E_4$ and d_{37}-$C_{18}E_4$) was purchased from Prof. Robert Thomas (Oxford University, UK). >99% pure deuterated alkanes were obtained from Aldrich and used without further purification.

PAN (MP = 3.5 °C) was prepared by reacting equimolar amounts of propylamine and conc. nitric acid to produce an aqueous solution, as described by Poole et al.[33] Excess water was removed by rotary evaporation followed by purging the concentrated PAN solution with nitrogen, and then heating at 110−120 °C for several hours under a nitrogen atmosphere. This leads to water contents undetectable by Karl Fischer titration (<0.01%) and prevents the formation of nitrous oxide impurities. Partially deuterated PAN (d_3-PAN) was prepared by performing the above reaction in D_2O rather than water. NMR revealed that, on average, this led to 2.5 of the three exchangeable hydrogens (bound to the nitrogen of the amine) being replaced with deuterium. This resulted in the scattering length density increasing from 1.1×10^6 A^{-2} for PAN to 2.6×10^6 A^{-2} for d_3-PAN.

Polarizing optical microscopy is a well-established technique for the detection of liquid crystal phases.[40−42] It relies on the fact the L_α and H_1 phases are anisotropic in structure, and consequently optically birefringent. When placed between crossed polarizers on an optical microscope stage, anisotropic media create distinct optical textures. The penetration or flooding experiments completed in this study used a small amount of nonionic between a microscope slide and a coverslip. PAN was then introducing from the coverslip edge and allowed to contact the surfactant by means of capillary action. The surfactant and

solvent slowly diffuse into one another, producing a roughly uniform concentration gradient.[42] In this way, the entire composition range can be quickly surveyed for the formation of liquid crystals. Selected samples were further characterized by small-angle X-ray scattering using a Bruker Nanostar equipped with a rotating anode source (Cu Kα, 1.541 Å), cross-coupled Göbel mirrors, three-pinhole collimation, and a Hi-Star 2D detector with 100 μm resolution, situated at ANSTO Lucas Heights.

Ternary phase diagrams were determined by weighing known amounts of surfactant into sample tubes and adding oil and PAN in a 1:1 mass ratio such that the total sample mass was 1 g. These samples were equilibrated at temperatures between 5 and ~95 °C in a water bath (±0.1 °C), and the number of phases present was recorded. This allows the phase boundaries to be determined. Samples were generally equilibrated for at least 24 h at each temperature because phases in these IL systems tended to separate slowly. As a result, we estimate the error in the position of the phase boundaries to be of the order of 1−2 °C. Previous investigations have shown that using deuterated species shifts the features of the phase diagram by only 1 or 2°C.[43]

SANS measurements were performed on freshly prepared samples using the LOQ spectrometer on the ISIS pulsed neutron source at the Rutherford Appleton Laboratory, U.K. The measurements determine the absolute scattering cross section $I(q)$ (cm^{-1}) as a function of a momentum transfer $q = (4\pi/\lambda)\sin(\theta/2)$, where λ is the incident neutron wavelength (2.2 Å $< \lambda <$ 10 Å) and θ the scattering angle. SANS data were collected using both the main detector bank and the high-angle detector bank, thus covering the range 0.008 Å$^{-1} < q <$ 1.4 Å^{-1}. The high and low q data sets were combined manually. Wavelength-dependent corrections were made for sample transmission, detector efficiencies, and incident spectrum. Normalization of the data to an absolute intensity scale was carried out by comparison to a known polymer standard[44] and a pure PAN background subtracted. A few low q data points were cut from each data set, and data for $q >$ 1 Å^{-1} was not used due to high levels of experimental error. One-dimensional $I(q)$ scattering spectra were imported into and analyzed using various fitting functions in the NIST Centre for Neutron Research Igor SANS analysis routines.[45]

Results and Discussion

C_iE_j/PAN Binary Phase Behavior. Table 1 summarizes the results of surfactant penetration scans of a range of nonionic surfactants with PAN. Both hexagonal (H_1) and lamellar (L_α) phases are commonly observed in addition to liquid isotropic (L_1) phases containing micellized surfactant dissolved in PAN (see below). Neither direct or inverse bicontinuous or discrete micellar cubic phases (V_1, V_2, or I_1) were observed in any of the binary systems examined. In contrast with ethylammonium nitrate (EAN) and water systems, we observed no cloud points in PAN for any of these surfactants at temperatures up to 65 °C. However, results on the microemulsion systems discussed below imply that many of these systems will exhibit lower consolute boundaries at higher temperatures.

The patterns of phase behavior of binary C_iE_j−PAN systems logically continue the progression observed in going from water to EAN as a polar solvent. First, the minimum alkyl chain lengths required to stabilize lyotropic phases is greater in PAN than EAN, which is in turn greater than in water. That is, the minimum alkyl chain length for which lyotropic phases are observed in PAN is $C_{16}E_j$, whereas $C_{14}E_4$ and $C_{14}E_8$ form lamellar and hexagonal phases, respectively, in EAN,[31] and

TABLE 1: Summary of Lyotropic Phases Observed in C_iE_j−PAN Binary Mixtures, Including the Melting Temperature (or Maximum Temperature Examined) of the Phase (Also Shown below the PAN Data Are the Corresponding Results in EAN[31] and Water,[46] Where Available)

		L_1	I_1	H_1	V_1	L_α	V_2	Int
$C_{14}E_4$	PAN	×						
	EAN					50 °C		
$C_{14}E_6$	PAN	×						
	EAN							
	H_2O			37 °C	40 °C	95 °C		
$C_{14}E_8$	PAN	×						
	EAN			30 °C				
$C_{16}E_4$	PAN	×				>65 °C		
	EAN					>60 °C		
	H_2O					74 °C	78 °C	
$C_{16}E_5$	PAN	×		22 °C		>65 °C		
$C_{16}E_6$	PAN	×		42 °C				
	EAN		40 °C	67 °C	48 °C			
	H_2O			34 °C	34 °C	102 °C		
$C_{16}E_8$	PAN	×		>65 °C				
	EAN			>60 °C				
	H_2O		12 °C	58 °C	62 °C	~106 °C		
$C_{18}E_3$	PAN	×						×
$C_{18}E_4$	PAN	×				×		
	EAN					>50 °C		
$C_{18}E_6$	PAN	×		>65 °C				
	EAN		35 °C	60 °C	56 °C	96 °C		
$C_{18}E_8$	PAN	×		44 °C				
	EAN		~40 °C	>60 °C	~50 °C	~60 °C		

$C_{10}E_{3-6}$ are well-known to form lyotropic phases in water that remain stable well above room temperature.[46] Second, there is a general trend toward stabilizing more highly curved aggregates progressing from water to EAN to PAN. Table 1 shows that, in both $C_{16}E_j$ and $C_{18}E_j$, hexagonal phases are stable in PAN to higher temperature at lower number of ethoxy groups compared to either EAN[31] or water.[46] This trend is also consistent with the previously noted[21,32] molecular volume of the alkylammonium cation responsible for the solvation of the hydrophilic polyoxyethylene chains, which should increase the molecular area of the amphiphile and lower the packing parameter.

One striking new feature observed in PAN is the existence of an intermediate phase of $C_{18}E_3$. The optical texture is inconsistent with either lamellar or hexagonal phases, resembling instead a mesh phase (cf. Figure A in the Supporting Information), as has been reported previously for nonionic surfactants with long alkyl chains.[47,48]

C_iE_j/PAN/Alkane Ternary Phase Behavior. Vertical sections through the phase prisms at equal masses of PAN and oil as a function of nonionic surfactant concentration are shown in Figure 1 and their characteristic values listed in Table 2. For all systems, the dimensions of the fish bodies are large and the minimum amount of surfactant required to form a single microemulsion phase is approximately 40 wt %. This is greater than those for EAN[32] or for similar aqueous[35,49,50] or formamide systems.[51] That is, the surfactant efficiency in PAN is low.

The existence of three-phase "fish" bodies implies that PAN microemulsions may form by a similar process to EAN, water, and formamide microemulsions in which the amphiphiles are more soluble in the polar solvent at low temperature, and in the oil at high temperature. Hence, they are expected to show similar structural progressions. However, the high temperatures of the upper limits of the three-phase region suggest that cloud points in PAN will be much higher than the range we investigated.

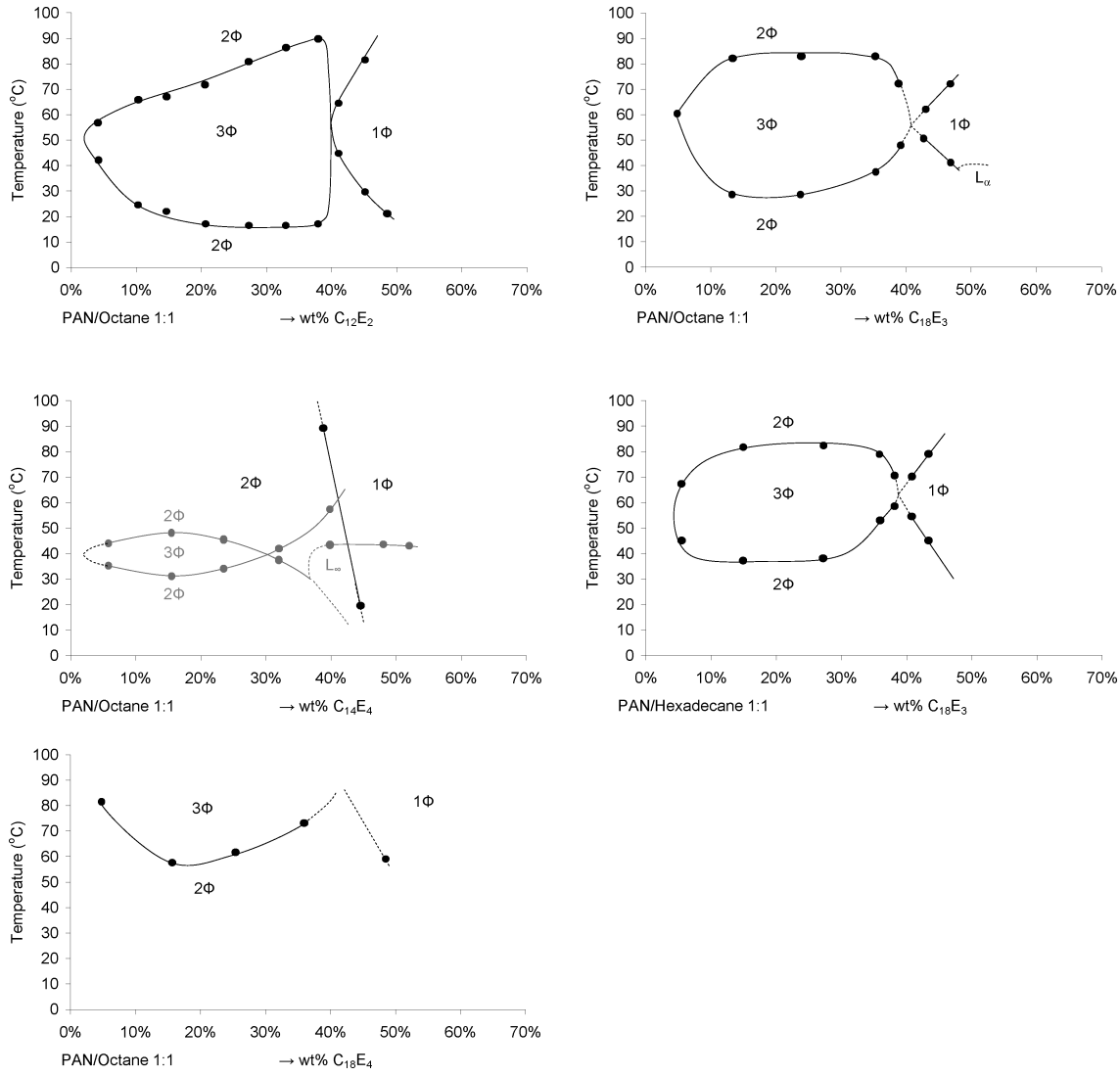

Figure 1. Vertical sections through the phase prisms for various PAN−C_iE_j−alkane systems. The corresponding EAN−$C_{14}E_4$−octane system is also shown (in gray) for comparison.

TABLE 2: Characteristic Values (ΔT, $\bar{T}$, and Surfactant Efficiency) for Phase Equilibria in C_iE_j−PAN−Alkane Microemulsions[a]

system	ΔT (°C)	$\bar{T}$ (°C)	surfactant efficiency, $\bar{X}$ (wt %)
$C_{12}E_2$−PAN−octane	64	52	40
$C_{18}E_3$−PAN−octane	54	54	40
$C_{18}E_3$−PAN−hexadecane	42	59	40
$C_{18}E_4$−PAN−octane		∼90	∼40

[a] $\bar{X}$ is defined by $\bar{T}$ and surfactant efficiency. The values for the $C_{18}E_3$−PAN−octane system are estimated from the portion of the phase diagram that was able to be determined.

A complete three-phase "fish" body for the $C_{14}E_4$−PAN−octane system could not be determined, as the surfactant remained dissolved in PAN up to the maximum accessible temperature. Only the position of the bottom portion of the "fish tail" separating the single microemulsion phase and two-phase regions was resolved. The balance temperature for the corresponding $C_{14}E_4$−EAN−octane system is much lower, at $\bar{T} = 40$ °C,[32] consistent with nonionic surfactants being more soluble in PAN than EAN. Similarly, the $C_{12}E_2$−octane−EAN system was not examined in our earlier study,[32] as its $\bar{T}$ was predicted to be below the freezing point of EAN around 5−10 °C, based on similar $C_{12}E_j$ amphiphiles in various alkanes. Comparing this with the observed $\bar{T}$ of 52 °C for $C_{12}E_2$−octane−PAN also indicates greater surfactant solubility in PAN. This solubility difference is likely a consequence of the longer alkyl tail of the propylammonium cation, which can lead to amphiphilic self-assembly in the pure IL.[19]

In aqueous,[35,49,50] formamide,[51] and ionic liquid microemulsions,[32] increasing surfactant amphiphilicity (simultaneously lengthening the headgroup and tailgroup) causes the fish size to first increase and then decrease. In water, the maximum occurs between C_5E_2 and C_6E_3, and between $C_{12}E_3$ and $C_{14}E_4$ in EAN, which is correlated with the microemulsion changing from weakly to strongly structured.[38] In strongly structured microemulsions, the conductivity decreases on warming as the continuous phase changes from polar through bicontinuous to nonpolar (oil), whereas the conductivity of weakly structured systems increases slightly due to decreasing viscosity. This transition was also demonstrated to occur in EAN microemulsions.[32] $C_{12}E_3$−EAN−dodecane microemulsions showed a monotonic increase in conductivity with temperature, whereas $C_{14}E_4$−EAN−dodecane decreased at temperatures greater than $\bar{T}$.

The conductivity of all PAN microemulsions shown in Figure 1 increased slightly with increasing temperature, up to temper-

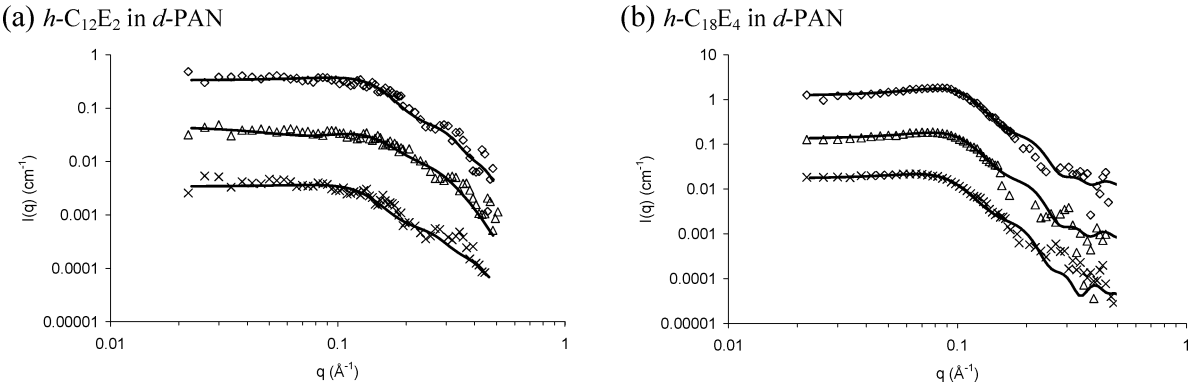

Figure 2. SANS scattering patterns for (a) 13 vol % h-$C_{12}E_2$ and (b) 14 vol % h-$C_{18}E_4$ in d-PAN, at 30 (◇), 45 (△), and 70 °C (×). Solid lines show fits combining a cylindrical form factor and hard sphere structure factor using the parameters listed in Table 3. For clarity, data at 45 and 75 °C are scaled by factors of 10 and 100, respectively.

atures far above $\bar{T}$, indicating that they are all weakly structured. This is initially surprising, as ΔT decreases by 10 °C between $C_{12}E_2$−PAN−octane and $C_{18}E_3$−PAN−octane. However, it does so with little or no change in either the balance temperature or, most tellingly, the surfactant efficiency (the position of $\bar{X}$). This, combined with our previous findings for EAN-based systems, leads us to suggest that weakly to strongly structured transition is indicated by an increase in surfactant efficiency, i.e., by $\bar{X}$ shifting to lower concentration with increasing amphiphilicity.

Overall, we find C_iE_j nonionic surfactants are less amphiphilic in PAN than in EAN, and less than in water. This does not preclude the possibility of strongly structured microemulsions in PAN but demonstrates the need to design or select surfactants that are more amphiphilic in ILs. This might be achieved by using Gemini[52,53] or fluorinated[54] nonionic surfactants or identifying an alternative polar moiety more soluble in the IL.

Increasing the alkane length (k) while the tailgroup (i) and headgroup (j) lengths are held constant lowers surfactant solubility in the oil, increasing the upper consulate temperature, while the cloud point in the polar solvent is unaffected. In aqueous[37] and EAN systems,[32] larger k increases ΔT and shifts $\bar{X}$ to higher temperatures and surfactant concentrations; i.e., $\bar{T}$ is increased and the fish body increases in size. Contrary to this expectation, increasing k from 8 to 16 with $C_{18}E_3$ reduces ΔT, while $\bar{X}$ is essentially unaffected. This cannot simply be attributed to weak microemulsion structure, as weakly structured aqueous systems respond as expected to variations in oil.[38] Rather, this is a consequence of the high surfactant solubility in PAN dominating over surfactant solubility changes in the oil. Increasing k from 8 to 16 causes the lower boundary of the fish body to shift to higher temperatures as expected. The reduction in ΔT and the invariance of $\bar{X}$ is due to the upper boundary remaining constant at ∼80 °C. Thus, the position of this boundary, which designates the point where all of the surfactant has moved from the middle phase into the oil, is determined entirely (within experimental error) by the solubility of the surfactant in PAN. The use of oils in which the surfactant is less soluble may produce the expected effect. Note that for EAN a marked effect for increasing k was only seen between 12 and 14; three-phase bodies for $k = 8$, 10, and 12 all had fairly similar features.[32]

In water-based systems, increasing headgroup size (j) increases the upper consolute temperature in the oil while simultaneously increasing the aqueous cloud point. This results in $\bar{T}$ being shifted to higher temperatures. As the cloud point increases more rapidly than the upper consolute temperature, the fish body grows larger (ΔT rises and $\bar{X}$ moves toward higher concentrations).[38,50] Previous results for the $C_{12}E_3$−EAN−dodecane and $C_{12}E_4$−EAN−dodecane systems showed the expected increases in $\bar{T}$ and ΔT, but the surfactant efficiency was unchanged.[32] Comparing $C_{18}E_3$−PAN−octane and $C_{18}E_4$−PAN−octane shows a similar dramatic increase in $\bar{T}$, while the surfactant efficiency is fairly similar in both systems. The effect on ΔT could not be ascertained. Preliminary SANS experiments for binary $C_{18}E_3$−PAN and $C_{18}E_4$−PAN systems (discussed below) suggested little difference in the solubility of these surfactants in PAN despite the different headgroup lengths. Therefore, the shift of the fish to higher temperatures must be due to lower solubility of the surfactant in octane as j is increased from 3 to 4.

Micellar Structure in Binary PAN−C_iE_j Systems. Scattering curves for a range of C_iE_j nonionic surfactants with $i = 12-18$ and $j = 2-4$ in PAN solution under a range of deuteration conditions and temperatures are shown in Figures 2−4. All show clear evidence of self-assembly into small micelles. Scattering from these solutions is modeled using a form factor $P(q)$ and an isotropically averaged structure factor, $S(q)$, according to

$$I(q) = N_P(V_{mic}\Delta\rho)^2 P(q)S(q) \quad (1)$$

where N_P is the number density of micelles and $\Delta\rho$ is the scattering length density difference (contrast) between the micelle and the solvent.[55] The data are fitted to either a cylindrical ($C_{12}E_2$, $C_{18}E_4$) or a polydisperse core−shell sphere form factor together with a hard sphere structure factor ($C_{14}E_4$, $C_{16}E_6$). For nonspherical micelles, the eccentricity is low and we expect the isotropic interaction approach to be adequate. Previous experiments employing similar surfactants and concentrations in EAN have shown that excluded volume (hard sphere) effects are sufficient to describe intermicelle repulsions.[56]

Scattering spectra for 13 vol % h-$C_{12}E_2$ in d_3-PAN as a function of temperature are shown in Figure 2a. The absolute scattered intensity is small, due primarily to the low contrast (cf. Table 3) between the scattering length densities of the hydrogenous surfactant (-3.7×10^{-7} Å^{-2} for the alkane and $+6.4 \times 10^{-7}$ Å^{-2} for the dry ethoxy headgroup) and d_3-PAN ($+2.5 \times 10^{-6}$ Å^{-2}). The surfactant concentration is high, and it is anticipated that most of the surfactant is aggregated into micelles, as cmc values for similar surfactants in EAN are of the order of 1 vol %.[21] The scattering data cannot be fit adequately to a model of either homogeneous or core−shell

TABLE 3: Sample Composition, Temperature, and Best Fit Parameters to SANS Data Using a Cylindrical Form Factor with Hard Sphere Structure Factor

	solvent	T (°C)	Φ_{actual}	$\Delta\rho$	Φ_{fit}	R (Å)	L (Å)	N_{agg}
h-$C_{12}E_2$	d_3-PAN	30	0.13	2.5×10^{-6}	0.15	19.5	9.0	50
		45	0.13	2.5×10^{-6}	0.135	20.0	9.0	52
		75	0.13	2.5×10^{-6}	0.13	23.0	7.0	54
h-$C_{18}E_4$	d_3-PAN	30	0.14	2.5×10^{-6}	0.18	26.7	19.2	83
		45	0.14	2.5×10^{-6}	0.17	27.2	19.8	89
		75	0.14	2.5×10^{-6}	0.15	30.1	20.5	112
d-$C_{18}E_4$	h-PAN	30	0.12	3.9×10^{-6}	0.18	24.0	20.0	70
d-$C_{18}E_4$	d_3-PAN	30	0.12	2.5×10^{-6}	0.19	24.1	20.9	74

spheres but are well described by short cylindrical (i.e., disk-like) micelles with excluded volume (equivalent hard sphere) interactions. The fitted length, or thickness, of the disks is only 9 Å, which is less than the fully extended length of a single C_{12} chain (16.7 Å), suggesting that the alkyl chains are intercalated and highly disordered within these micelles. The micelle radius at 30 °C is 19.5 Å, slightly longer than a C_{12} chain but about 20% less than the length of a fully extended $C_{12}E_2$ (25.5 Å). Previous studies of nonionic micelles in EAN have shown that the ethoxy headgroups are strongly solvated, so that they are nearly contrast-matched to the IL solvent.[21] This means that this scattering is sensitive to the hydrocarbon core dimensions, which are also smaller than the fully extended dodecyl chains in EAN. This has been attributed to a weaker solvophobic effect for alkyl chains in EAN than water, which should be weaker still in PAN.

The micelle aggregation number, N_{agg}, is determined by dividing the micelle core volume ($\pi R^2 l$) by the volume of a single C_{12} moiety (350 Å^3), yielding 50 at 30 °C. When the temperature is increased to 45 and 75 °C, the disk radius increases slightly, yielding a modest increase in aggregation number. Increasing temperature reduces the extent of H-bonding between the surfactant headgroup and PAN, as seen in both aqueous[46] and EAN systems.[31] This decreases the curvature of the micelle (increased surfactant packing parameter), favoring larger disks as observed. Disk-like micelles are also observed for 14 vol % h-$C_{18}E_4$ in d-PAN, and the thickness of these, too, is less than a single, all-*trans* octadecyl chain (24.3 Å), while the radius is only slightly greater. Again, assuming these to be micelle core dimensions yields an aggregation number of 83, which increases to 112 as the disk radius grows on warming to 75 °C.

For both $C_{12}E_2$ and $C_{18}E_4$, the fitted micelle volume fractions are greater than expected. This is due in part to the use of an effective hard sphere repulsion to describe interactions between anisotropic micelles, and also to solvation of the headgroup layer by PAN. The fitted volume fraction exceeds the "dry" volume fraction by more for $C_{18}E_4$ than for $C_{12}E_2$, even though these are less eccentric. Solvation is thus the more important factor and its effect greater for longer ethoxy chains. The fitted micelle volume fraction decreases on warming in both systems, although the micelles become more disk-like, also implicating solvation as the major influence on volume fraction. By comparison, $C_{18}E_6$ forms elongated cylindrical micelles between 1 and 20 wt % in

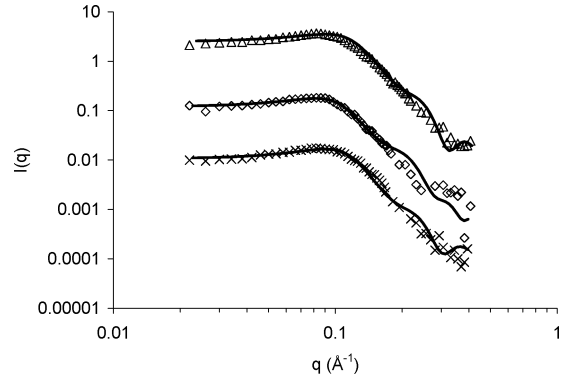

Figure 3. SANS scattering spectra at 30 °C for 14 vol % d-$C_{18}E_4$ in h-PAN (△), 14 vol % h-$C_{18}E_4$ in d-PAN (◇), and 12 vol % d-$C_{18}E_4$ in d-PAN (×). Solid lines show fits combining a cylindrical form factor and hard sphere structure factor using the parameters listed in Table 3.

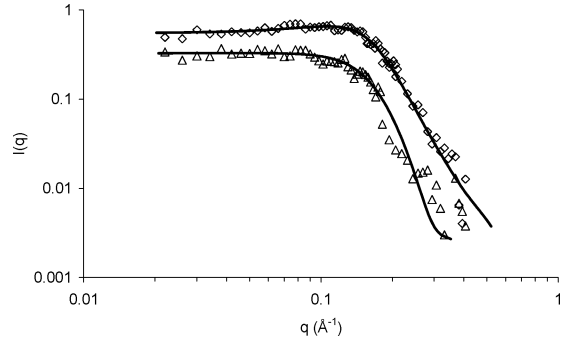

Figure 4. SANS scattering spectra at 30 °C for 11 vol % d-$C_{14}E_4$ in h-PAN (◇) and 7 vol % h-$C_{16}E_6$ in d_3-PAN (△). Solid lines show fits combining a polydisperse core−shell form factor and hard sphere structure factor using the parameters listed in Table 4.

EAN with a short core dimension radius of between 20 and 24.3 Å as expected for an octadecyl tail. The formation of cylinders there is consistent with the larger ethoxy headgroup.

A comparison of the scattering obtained from $C_{18}E_4$ in PAN at three different contrasts is shown in Figure 3 at 30 °C, together with fits to interacting cylindrical disks. Note that the d_{37}-$C_{18}E_4$/d_3-PAN system does not describe shell or film contrast: The contrast primarily arises from the difference between the scattering length density of the tail deuteration of the monomer (5.0×10^{-6} Å^{-2}) and the partially deuterated solvent (2.5×10^{-6} Å^{-2}). Within experimental uncertainty, the fitted parameters obtained for this system are identical for all isotopic compositions (Table 3).

SANS spectra of 11 vol % d_{29}-$C_{14}E_4$ in h-PAN and 7 vol % h-$C_{16}E_6$ in d_3-PAN are shown in Figure 4. Scattering from $C_{14}E_4$ is well described as slightly polydisperse, globular, core−shell micelles in PAN. The polydispersity may indicate a modest eccentricity in micelle shape, which would be indistinguishable in the scattering pattern. The micelle core radius of 11.2 Å (Table 4) is markedly smaller than an extended tetradecyl chain (19 Å), and the aggregation number is correspondingly low at 15. Both values accord with the radius of 14 Å and aggregation number of 17 determined for tetradecylpyridinium bromide in

TABLE 4: Sample Composition and Best Fit Parameters to SANS Data Using a Polydisperse Core−Shell Sphere Form Factor with Hard Sphere Structure Factor at 30 °C

	solvent	Φ_{actual}	Φ_{fit}	R_c (Å)	ρ_{core}	t_{shell} (Å)	ρ_{shell}	polydispersity	N_{agg}
d-$C_{14}E_4$	h-PAN	0.11	0.13	11.2	7.08×10^{-6}	5.6	6.50×10^{-7}	0.28	15
h-$C_{16}E_6$	d-PAN	0.07	0.08	14.1	-3.5×10^{-7}	3.5	2.46×10^{-6}	0.17	26

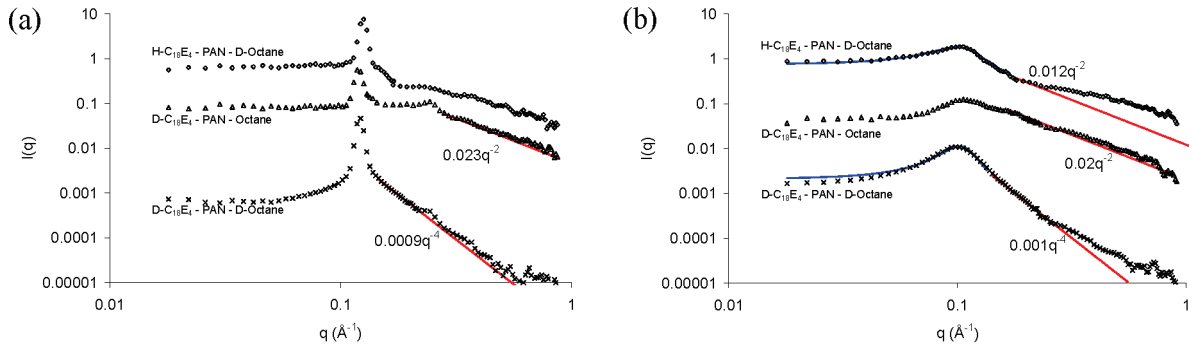

Figure 5. SANS spectra for 50 wt % d_{37}-$C_{18}E_4$−PAN−*d*-octane (×), *h*-$C_{18}E_4$−PAN−*d*-octane (◇), and d_{37}-$C_{18}E_4$−PAN−*h*-octane (△) with the incoherent background subtracted at (a) 30 °C and (b) $\bar{T} = 90$ °C, showing fits to the TS model. For clarity, the intensities for d_{37}-$C_{18}E_4$−PAN−*h*-octane and d_{37}-$C_{18}E_4$−PAN−*d*-octane have been scaled by factors of 0.1 and 0.001, respectively.

EAN.[24] As inferred above, the fitted scattering length density of the shell is close to that of the solvent, indicating a high degree of solvation of the ethoxy groups by PAN, and the fitted volume fraction correspondingly larger than the "dry" surfactant.

The globular micelle shape is consistent with the increased headgroup/tail volume ratio for this surfactant compared to $C_{12}E_2$ and $C_{18}E_4$ above, and with previous reports for both aqueous and EAN systems, but is quite different from EAN in which $C_{14}E_4$ forms elongated cylinders.[21] This may be due to the greater solvation volume of the ethoxylate head groups associated with propyl- rather than ethylammonium cations. Another possibility is the incorporation of alkylammonium ions as cosurfactants in micelles, which has been suggested previously.[57] There is certainly good evidence that these ions act as amphiphiles in the pure ionic liquid,[19] so cosurfactancy is plausible, and more likely for propyl- than ethylammonium salts. In this light, it is tempting to speculate whether the smaller disk radii observed in d_{37}-$C_{18}E_4$ than those in *h*-$C_{18}E_4$ (Table 3) might be due to the incorporation of hydrogenous propyl tails in the curved edges of the micellar disks.

SANS scattering data for 7 vol % *h*-$C_{16}E_6$ in *d*-PAN reveals that this surfactant also forms globular micelles with a strongly solvated, weakly contrasting headgroup layer. The core radius (14 Å) is once again substantially less than the length of a fully extended hexadecyl chain (22 Å) and the micelle aggregation number correspondingly low. Both values again compare quite well with light scattering results for hydrodynamic radius (22 Å) and aggregation number (26) of hexadecylpyridinium bromide micelles in EAN.[24]

Structure in Ternary Systems: $C_{18}E_4$−PAN−Octane. Figure 5 shows SANS spectra for the $C_{18}E_4$−PAN−octane system (see Figure 1) in both the lamellar phase and balanced microemulsion ($\bar{T}$) at three different scattering contrasts: d_{37}-$C_{18}E_4$−PAN−*d*-octane, *d*-$C_{18}E_4$−PAN−*h*-octane, and *h*-$C_{18}E_4$−PAN−*d*-octane. Hydrogenous PAN has been used throughout the studies of ternary systems, as its scattering length density ($\rho = 1.1 \times 10^{-6}$ Å^{-2}) is quite different from other hydrogenous and deuterated components, as discussed below.

In the lamellar phase at 30 °C, the scattering for all three contrasts is dominated by a sharp Bragg peak at $q = 0.126$ Å^{-1}. Higher order peaks are also evident in some cases at $q = 0.25$ Å^{-1}. The primary peak position corresponds to a repeat spacing $D^* = 2\pi/q_{max}$ of 50 Å. Using molecular volumes, the polar (surfactant headgroup + PAN) and apolar (surfactant tails + oil) volume fractions are 0.38 and 0.62, which partitions the lamellar phase into polar and apolar regions 19 and 31 Å thick. As the calculated lengths of the $C_{18}E_4$ headgroups (16 Å) and alkyl tails (24 Å) are significantly greater than half of these thicknesses, the heads and tails must either be highly interdigitated within the domain or contain a substantial number of gauche rotamers. The form of the scattering at high *q* favors the former explanation.

The scattering from the d_{37}-$C_{18}E_4$−PAN−*d*-octane lamellar phase at high *q* decays as q^{-4}, consistent with a sharp interface separating deuterated nonpolar and hydrogenous polar regions.[58] This is also consistent with strong solvation of the ethoxylated headgroup by the IL, as observed in the binary systems using d_3-PAN in which the headgroup layer contributes negligible scattering contrast against the bulk solvent. That is, the polar regions can be treated as having homogeneous scattering length densities. Apart from a small deviation at very high *q*, the same behavior is observed in the balanced microemulsion.

Strikingly however, the high *q* scattering from both the *h*-$C_{18}E_4$−PAN−*d*-octane and d_{37}-$C_{18}E_4$−PAN−*h*-octane systems decay much more gradually, approximating a q^{-2} dependence expected for film contrast.[58] This behavior can only arise if the octane and the alkyl chains of the surfactant are almost completely segregated from each other within the microemulsion. The d_{37}-$C_{18}E_4$−PAN−*h*-octane system necessarily gives rise to film-contrast scattering thanks to the high scattering length density of the deuterated C_{18} chains that separate the hydrogenous octane and PAN. Even very high uptake of hydrogenous octane would still give a core−shell or film-like scattering length density profile. However, even slight penetration of *d*-octane ($\rho = 6 \times 10^{-6}$ Å^{-2}) into the hydrogenous alkyl tails ($\rho = -0.5 \times 10^{-6}$ Å^{-2}) of the *h*-$C_{18}E_4$−PAN−*d*-octane system would raise the film scattering length density enough to lead to a gradual change in scattering length density profile through the surfactant-coated film from *d*-octane to the *h*-PAN/ethoxylate polar region ($\rho = 0.5 \times 10^{-6}$ Å^{-2}). Such a scattering length density profile fails to describe the observed scattering behavior, as this would cause the high *q* scattering to fall off faster than q^{-4}.[58,59] The conclusion that the oil and alkyl tails of the surfactant are almost completely segregated seems unavoidable.

When temperature is increased, a structural transition from lamellar to microemulsion occurs. The scattering peak becomes broader and less intense and moves toward lower *q* as the disorder and characteristic length of the system increase. As observed with the lamellar phase, the scattering from the d_{37}-$C_{18}E_4$−PAN−*d*-octane system is consistent with a sharp interface between polar and apolar domains, but both other scattering contrasts exhibit film-like high-*q* behavior. We therefore deduce that the segregation of octane from the alkyl chains persists in the microemulsions.

Scattering from d_{37}-$C_{18}E_4$−PAN−*d*-octane may be fit using the Teubner−Strey (TS) model, which has been widely used to describe scattering from aqueous[59−61] and EAN[32] microemul-

TABLE 5: Best-Fit Values of d (Å) as a Function of T (°C) for Mixtures of 50 wt % C_iE_j, 25 wt % PAN, and 25 wt % d-Octane

T (°C)	$C_{12}E_2$	$C_{14}E_4$	$C_{18}E_3$	$C_{18}E_4$	D-$C_{18}E_4$
45	49.8	52.3	54		
50			54.8	54.7	53.8
60	52.7	52.9	56.3	55.5	54.8
70			58.5	56.4	56.0
75	57.1	55.1			
90	65.3	58.0	65	59.8	60.0

sions with a sharp interface between polar and apolar domains. This model uses three fitting parameters to describe the scattering in terms of two characteristic lengths, the periodicity of the polar and nonpolar domains, d, and a correlation length, ξ, which describes the decay of that periodic order. The scattering function has the general form[61]

$$I(q) = \frac{1}{a_2 + c_1q^2 + c_2q^4} \tag{2}$$

with ξ and d given by

$$\xi = \left[\frac{1}{2}\left(\frac{a_2}{c_2}\right)^{1/2} + \frac{1}{4}\frac{c_1}{c_2}\right]^{-1/2}, \frac{d}{2\pi} = \left[\frac{1}{2}\left(\frac{a_2}{c_2}\right)^{1/2} - \frac{1}{4}\frac{c_1}{c_2}\right]^{-1/2} \tag{3}$$

The ratio d/ξ has been described as a measure of the polydispersity of the polar and nonpolar domains,[62] and is found to be near 2 for many aqueous microemulsions near $\bar{X}$.[59] For EAN microemulsions, the lower surfactant efficiency leads to higher minimum surfactant concentrations, and to smaller d and ξ. However, we also found $1 < d/\xi < 1.5$, indicating more ordered structures in which spatial correlation persisted over more oil/EAN domains.

Fits of the Teubner−Strey model to scattering spectra of $C_{18}E_4$−PAN−octane at three scattering contrasts at $\bar{T}$ (90 °C) are shown in Figure 5, and the best-fit values of d as a function of temperature are reported in Table 5. Both the peak position and peak widths are similar for both contrasts, but the intensity of the d_{37}-$C_{18}E_4$−PAN−d-octane system is substantially higher due to the greater deuterated volume. The best-fit values of d are the same within experimental uncertainty for the two contrasts, as might be expected from the similarity of the position of q_{max}. Conversely, ξ values were much lower for the hydrogenated surfactant system, even when the fit is constrained to only function in the vicinity of the peak. The high-q scattering evidently distorts the scattering function toward an apparently broader and lower peak, whence a lower apparent ξ. That is, the scattered intensity that is expected to be present at intermediate q is manifested at high q. As a result, ξ values obtained with hydrogenous surfactants and deuterated oils have no physical meaning in terms of microemulsion structure and are not reported, but the fitted d values in the hydrogenous surfactant systems are quite reliable.

The results for PAN systems are consistent with previous observations on EAN microemulsions. The fitted periodicities are small, and in the range expected for low surfactant efficiencies. In D-$C_{18}E_4$−PAN−D-octane, the ξ values indicate a high degree of order.

Interfacial Molecular Areas. The molecular area occupied by a surfactant at the oil/PAN interface can be obtained, in the case of a sharp interface, from Porod analysis[63] of bulk contrast SANS. The area density, S/V, is obtained from[64]

$$\frac{S}{V} = \frac{\pi \lim_{q\to\infty}[q^4I(q)]}{Q^*} \tag{4}$$

where Q^* is the scattering invariant $Q^* = \int_0^\infty q^2I(q)\,dq = 2\pi^2(\Delta\rho)^2\Phi(1-\Phi)$, $\Delta\rho$ is the scattering contrast, and Φ is the volume fraction of one of the contrasting components. The area per molecule, a_s, is then obtained from the composition, assuming that all surfactant molecules are located at the interface. In PAN systems, this may lead to a_s being underestimated by a few percent. The values obtained for Q^* by numerical integration of the scattered intensities were within a few percent of those determined from sample compositions, providing high levels of data confidence.

In the lamellar phase, the molecular area can also be calculated from the peak position by geometrical considerations using

$$a_s = \frac{2v_s}{D^*\Phi_s} \tag{5}$$

where Φ_s is the volume fraction of surfactant and its molecular volume $v_s = M\rho_s^{-1}N_a^{-1}$ is determined from its density (ρ_s) and molecular weight (M).

TABLE 6: Area per Molecule (a_s) in the Microemulsion and Lamellar Phases

system	T (°C)	phase	S/V (Å^{-1})	a_s (Å^2)
d_{37}-$C_{18}E_4$−PAN−h-octane	30	lamellar		68[a]
d_{37}-$C_{18}E_4$−PAN−d-octane	30	lamellar	0.041	67, 65[a]
	50	microemulsion	0.053	91
	60	microemulsion	0.052	88
	70	microemulsion	0.045	86
	90	microemulsion	0.046	77

[a] Determined from the repeat spacing using eq 5.

Molecular areas in the lamellar and microemulsion phases obtained by both methods are presented in Table 6. Results for the lamellar phase at 30 °C obtained by the two methods are in excellent agreement, as are the areas obtained from eq 5 using different scattering contrasts. The average molecular area of 67 Å^2 is substantially greater than either the 50 Å^2 observed for $C_{14}E_4$−EAN−dodecane[32] or even the 42.9 Å^2 for the $C_{12}E_5$−water−octane microemulsions.[60] Neither the size of the surfactant tailgroup or the length of the alkane substantially affect a_s,[59] which is primarily determined by the size and conformation of the surfactant headgroup and the species that hydrogen bond to it. We conclude, therefore, that the greater molecular volume of propylammonium compared to ethylammonium or water solvating the ethoxy chains is responsible for the larger molecular area.

a_s increases abruptly from 67 to 91 Å^2 as the structure changes from lamellar at 30 °C to microemulsion at 50 °C, and then remains fairly constant between 50 and 70 °C before decreasing again to 77 Å^2 at the balance temperature of 90 °C. This is due to decreased hydrogen bonding between the ionic liquid and the headgroup as temperature is increased, which lowers the amount of PAN bound to the surfactant headgroup and decreases steric repulsions. Similar results have been observed for EAN microemulsions.[32] Over the same temperature interval, d

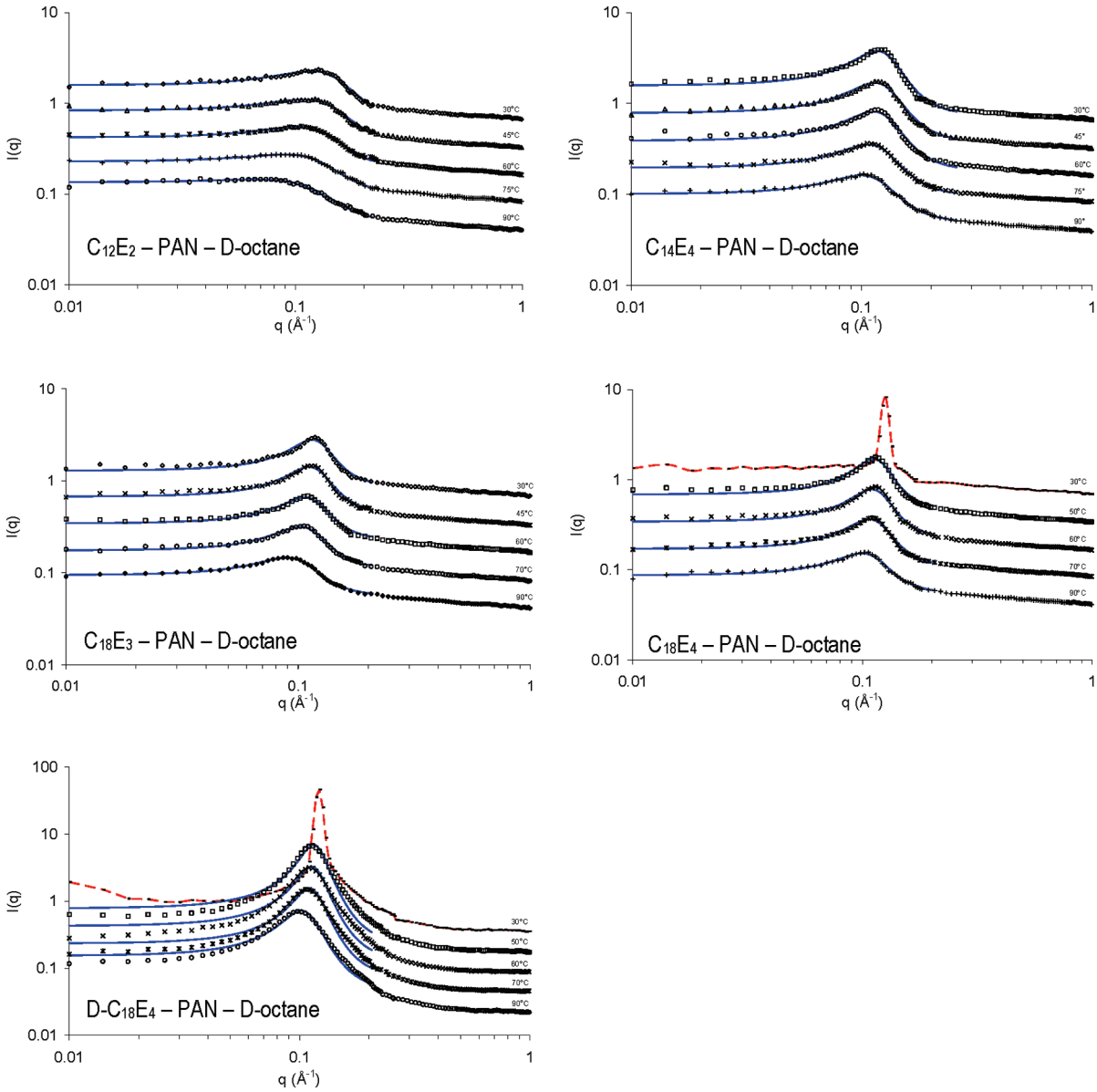

Figure 6. SANS spectra for 50 wt % C_iE_j with 25 wt % PAN and 25 wt % oil as a function of temperature, showing $\bar{T}$ for each system (approximated by 90 °C for $C_{18}E_4$−octane−PAN). For clarity, each intensity has been multiplied by a factor of 0.5 as the temperature increases. The solid lines are fits obtained using the Teubner−Strey model + background. The dashed lines for the lamellar spectra are to guide the eye. Two contrasts are shown for the $C_{18}E_4$ system.

increases gradually (Table 5) as the average surfactant layer curvature is reduced. ξ also decreases with increasing temperature as thermal fluctuations increase.

These molecular areas are all 3−4 times larger than individual alkyl chain cross sections, and this points to possible reasons for the segregation between oil and alkyl tails observed in the scattering patterns. Either the octane must penetrate the alkyl tails right up to the PAN, accounting for 66−75% of the film volume, or else the alkyl chains must contain many *gauche* rotamers, covering most of the interface and excluding the oil. Such an oil-rich interfacial film seems contrary to the formation of a microemulsion. One further possibility is that the propylammonium acts as a cosurfactant and occupies some of the space between amphiphiles with the propyl moieties oriented into the nonpolar regions. This would account for the high molecular areas, and would also be consistent with the observed film-contrast scattering in the *d*-octane−*h*-$C_{18}E_4$−PAN systems.

Effect of Surfactant on Microemulsion Structure. SANS spectra for C_iE_j−PAN−octane systems with equal masses of oil and PAN between 30 and 90 °C are shown in Figure 6, together with best fits to the Teubner−Strey model. The values of d (and of ξ and d/ξ for the $C_{18}E_4$−PAN−octane mixtures) obtained from Teubner−Strey fits to the spectra shown in Figures 5 and 6 are listed in Table 5. Porod analysis and ξ values are not reported for mixtures that employed hydrogenous surfactant, as these exhibit significant film-like high q scattering.

A single broad scattering peak is observed for all mixtures at all temperatures, except for the $C_{18}E_4$ system where sharp lamellar peaks occur at low temperature, as detailed above. Simple inspection of Figure 6 shows that the microemulsion scattering peak is more distinct for larger surfactants, showing a higher degree of order. This effect is most noticeable between $C_{12}E_2$ and $C_{14}E_4$, but the progression continues when comparing spectra at $\bar{T}$ (Table 2). Small changes in peak position between balanced surfactants can be mostly attributed to small differences in surfactant volume fractions (see Table 7).

TABLE 7: Volume Fraction of Surfactant Θ, $I(q)_{max}$, and q_{max} Values for C_iE_j−PAN−*d*-Octane Mixtures

system	Θ C_iE_j	q_{max} (cm^{-1})	$I(q)_{max}$ (cm^{-1})
$C_{12}E_2$−PAN−*d*-octane	51%	0.94	1.6
$C_{14}E_4$−PAN−*d*-octane	53%	0.118	2.8
$C_{18}E_3$−PAN−*d*-octane	51%	0.102	2.1
$C_{18}E_4$−PAN−*d*-octane	52%	0.102	1.9

A remarkable result of the model fitting is that the periodicity, *d*, is almost the same at each temperature (Table 5), showing the limited effect of surfactant structure on interfacial area.

For all surfactants, the scattering peak becomes broader and less intense, while q_{max} decreases and the corresponding best-fit value of *d* increases, as temperature is increased. The increase in *d* is a consequence of the surfactant film area decreasing; Table 6 shows that the area per surfactant molecule decreases with temperature. The higher temperature also increases thermal disorder, broadening the scattering peak.

Conclusions

PAN supports the full range of amphiphilic self-assembly behavior of nonionic surfactants into micelles, lyotropic liquid crystals, and microemulsions. Ethylene oxide head groups are strongly solvated by PAN, as reported for EAN,[21,31,32] but the longer propyl moiety also increases the solubility of the surfactant, by increasing alkyl chain solubility. This means that longer surfactant tail groups are needed in order to form lyotropic phases in PAN than either EAN or water, and also that surfactant efficiency in microemulsion formation is lower in PAN than EAN or water. Strong solvation, together with the greater molecular volume of PAN results in higher molecular areas in the self-assembled aggregates. This is verified by geometrical model fits and Porod limit scattering behavior. This favors a smaller surfactant packing parameter or more highly curved aggregates in PAN than EAN or water.

Although no cloud points were detected for any nonionic surfactant in PAN, ternary phase behavior parallels that of EAN- and water-based systems. This suggests that surfactant solubility should decrease in PAN on warming, and is supported by the decreasing molecular areas observed on warming in PAN microemulsions. Phase behavior and conductivity reveal that C_iE_j−PAN−oil microemulsions are all weakly structured for the surfactants investigated up to $C_{18}E_j$. Changing oils from octane to hexadecane had little effect on ternary phase behavior. Increasing surfactant amphiphilicity only marginally increased microemulsion efficiency but does cause an increase in the neutron scattering peak intensity, suggesting greater order within the system. Only the longest alkyl chains investigated displayed a ternary lamellar phase adjacent to the microemulsion. These results are all attributed to high surfactant solubility in the ionic liquid.

Throughout these studies, there have been frequent indications that the propylammonium ion may act as a cosurfactant in self-assembled structures in PAN. The stability of disk-like micelles, the high curvature of all of the aggregates formed, the high molecular area in microemulsions and lamellar phases, and even the unusual film-contrast scattering from *h*-$C_{18}E_4$−PAN−*d*-octane are all at least consistent with incorporation of a short alkyl-chained cosurfactant. This idea also gels with independent evidence of self-assembly of pure PAN and, to a lesser extent, EAN in the bulk and at interfaces.[15,19,65,66] Decisive evidence will require a separate and specifically designed study.

The low efficiency of conventional nonionic surfactants in PAN means that high surfactant concentrations are required for self-assembly to occur, and to solubilize the polar and apolar phases into a single microemulsion. Methods for increasing surfactant efficiency in ILs will be necessary before full exploitation of ionic liquids in self-assembly will be possible.

Acknowledgment. This work was funded by the Australian Research Council through Discovery Grant (DP0986194). R.A. thanks the University of Newcastle for a Research Fellowship. Experiments at the ISIS Pulsed Neutron and Muon Source were supported by a beamtime allocation from the Science and Technology Facilities Council. We thank Dr Richard Heenan for his assistance with the SANS experiments and data reduction. Travel to ISIS was funded through the Access to Major Research Facilities Program administered by ANSTO.

Supporting Information Available: Figure showing the optical texture of $C_{18}E_3$ in PAN at 25 °C. This material is available free of charge via the Internet at http://pubs.acs.org.

References and Notes

(1) Seddon, K. R.; Stark, A.; Torres, M. J. *Pure Appl. Chem.* **2000**, *72*, 2275.
(2) Welton, T. *Chem. Rev.* **1999**, *99*, 2071.
(3) Forsyth, S. A.; Pringle, J. M.; MacFarlane, D. R. *Aust. J. Chem.* **2004**, *57*, 113.
(4) Greaves, T. L.; Weerawardena, A.; Fong, C.; Drummond, C. J. *Langmuir* **2007**, *23*, 402.
(5) Evans, D. F.; Yamauchi, A.; Roman, R.; Casassa, E. Z. *J. Colloid Interface Sci.* **1982**, *88*, 89.
(6) Belieres, J. P.; Angell, C. A. *J. Phys. Chem. B* **2007**, *111*, 4926.
(7) Greaves, T. L.; Weerawardena, A.; Fong, C.; Drummond, C. J. *J. Phys. Chem. B* **2007**, *111*, 4082.
(8) Greaves, T. L.; Weerawardena, A.; Fong, C.; Krodkiewska, I.; Drummond, C. J. *J. Phys. Chem. B* **2006**, *110*, 22479.
(9) Gordon, J. E.; Rao, G. N. S. *J. Am. Chem. Soc.* **1978**, *100*, 7445.
(10) Sun, J.; Forsyth, M.; MacFarlane, D. R. *J. Phys. Chem. B* **1998**, *102*, 8858.
(11) Bloom, H.; Reinsborough, V. C. *Aust. J. Chem.* **1969**, *22*, 519.
(12) Noda, A.; Hayamizu, K.; Watanabe, M. *J. Phys. Chem. B* **2001**, *105*, 4603.
(13) Brookes, R.; Davies, A.; Ketwaroo, G.; Madden, P. A. *J. Phys. Chem. B* **2005**, *109*, 6485.
(14) Aerov, A. A.; Khokhlov, A. R.; Potemkin, I. I. *J. Phys. Chem. B* **2006**, *110*, 16205.
(15) Atkin, R.; Warr, G. G. *J. Phys. Chem. C* **2007**, *111*, 5162.
(16) Horn, R. G.; Evans, D. F.; Ninham, B. W. *J. Phys. Chem.* **1988**, *92*, 3531.
(17) Carmichael, A. J.; Hardacre, C.; Holbrey, J. D.; Nieuwenhuyzen, M.; Seddon, K. R. *Anal. Chem.* **1999**, *71*, 4572.
(18) Triolo, A.; Russina, O.; Bleif, H. J.; DiCola, E. *J. Phys. Chem. B* **2007**, *111*, 4641.
(19) Atkin, R.; Warr, G. G. *J. Phys. Chem. B* **2008**, *112*, 4164.
(20) Anderson, J. L.; Pino, V.; Hagberg, E. C.; Sheares, V. V.; Armstrong, D. W. *Chem. Commun.* **2003**, 2444.
(21) Araos, M. U.; Warr, G. G. *Langmuir* **2008**, *24*, 9354.
(22) Bowlas, C. J.; Bruce, D. W.; Seddon, K. R. *Chem. Commun.* **1996**, 1625.
(23) Evans, D. F.; Yamauchi, A.; Roman, R.; Casassa, E. Z. *J. Colloid Interface Sci.* **1982**, *88*, 89.
(24) Evans, D. F.; Yamauchi, A.; Wei, G. J.; Bloomfield, V. A. *J. Phys. Chem.* **1983**, *87*, 3537.
(25) Firestone, M. A.; Dzielawa, J. A.; Zapol, P.; Curtiss, L. A.; Seifert, S.; Dietz, M. L. L. *Langmuir* **2002**, *18*, 7258.
(26) Fletcher, K. A.; Pandey, S. L. *Langmuir* **2004**, *20*, 33.
(27) Gordon, C. M.; Holbrey, J. D.; Kennedy, A. R.; Seddon, K. R. J. M. C. *J. Mater. Chem.* **1998**, *8*, 2627.
(28) Yoshio, M.; Mukai, T.; Kanie, K.; Yoshizawa, M.; Ohno, H.; Kato, T. *Chem. Lett.* **2002**, 320.
(29) Beesley, A. H.; Evans, D. F.; Laughlin, R. G. *J. Phys. Chem.* **1988**, *92*, 791.
(30) Atkin, R.; Warr, G. G. *J. Am. Chem. Soc.* **2005**, *127*, 11940.
(31) Araos, M. U.; Warr, G. G. *J. Phys. Chem. B* **2005**, *109*, 14275.
(32) Atkin, R.; Warr, G. G. *J. Phys. Chem. B* **2007**, *111*, 9309.
(33) Poole, C. F.; Kersten, B. R.; Ho, S. S. J.; Coddens, M. E.; Furton, K. G. *J. Chromatogr., A* **1986**, *352*, 407.
(34) Xiao, D.; Rajian, J. R.; Cady, A.; Li, S.; Bartsch, R. A.; Quitevis, E. L. *J. Phys. Chem. B* **2007**, *111*, 4669.

(35) Kahlweit, M.; Strey, R.; Firman, P.; Haase, D.; Jen, J.; Schomacker, R. *Langmuir* **1988**, *4*, 499.
(36) Auvray, L.; Cotton, J. P.; Ober, R.; Taupin, C. *J. Phys. Chem.* **1984**, *88*, 4586.
(37) Kahlweit, M.; Strey, R.; Busse, G. *J. Phys. Chem.* **1990**, *94*, 3881.
(38) Kahlweit, M.; Strey, R.; Busse, G. *Phys. Rev. E* **1993**, *47*, 4197.
(39) Schubert, K. V.; Busse, G.; Strey, R.; Kahlweit, M. *J. Phys. Chem.* **1993**, *97*, 248.
(40) Rosevear, F. B. *J. Am. Oil Chem. Soc.* **1954**, *31*, 628.
(41) Rosevear, F. B. *J. Soc. Cosmet. Chem.* **1968**, *19*, 581.
(42) Laughlin, R. G. *The Aqueous Phase Behavior of Surfactants*; Academic Press: London, 1994.
(43) Endo, H.; Mihailescu, M.; Monkenbusch, M.; Allgaier, J.; Gompper, G.; Richter, D.; Jakobs, B.; Sottmann, T.; Strey, R.; Grillo, I. *J. Chem. Phys.* **2001**, *115*, 580.
(44) Heenan, R. K.; Penfold, J. P.; King, S. M. *J. Appl. Crystallogr.* **1997**, *30*, 1140.
(45) Kline, S. R. *J. Appl. Crystallogr.* **2006**, *39*, 895.
(46) Mitchell, D. J.; Tiddy, G. J. T.; Waring, L.; Bostock, T.; McDonald, M. P. *J. Chem. Soc., Faraday Trans. 1* **1983**, *79*, 975.
(47) Burgoyne, J. H.; M, C.; Tiddy, G. J. T. *J. Phys. Chem.* **1995**, *99*, 6054.
(48) Funari, S. S.; H, M. C.; Tiddy, G. J. T. *J. Phys. Chem.* **1992**, *96*, 11029.
(49) Kahlweit, M.; Strey, R.; Firman, P. J.; Haase, D. *Langmuir* **1985**, *1*, 281.
(50) Kahlweit, M.; Strey, R.; Firman, P. *J. Phys. Chem.* **1986**, *90*, 671.
(51) Schubert, K. V.; Strey, R. *J. Chem. Phys.* **1991**, *95*, 8532.
(52) Fitzgerald, P. A.; Carr, M. W.; Davey, T. W.; Serelis, C. H.; Such, C. H.; Warr, G. G. *J. Colloid Interface Sci.* **2004**, *275*, 649.
(53) Fitzgerald, P. A.; Davey, T. W.; Warr, G. G. *Langmuir* **2005**, *21*, 7121.
(54) Davey, T. W.; Warr, G. G.; Almgren, M.; Asakawa, T. *Langmuir* **2001**, *17*, 5283.
(55) Hayter, J. B. *Physics of Amphiphiles: Micelles, Vesicles, and Microemulsions*; Degiorgio, V., Corti, M., Eds.; Elsevier Science: New York, 1983.
(56) Lum Wan, J. A.; Warr, G. G.; White, L. R.; Grieser, F. *Colloid Polym. Sci.* **1988**, *265*, 528.
(57) Evans, D. F.; Kaler, E. W.; Benton, W. J. *J. Phys. Chem.* **1983**, *87*, 533.
(58) Strey, R.; Winkler, J.; Magid, L. *J. Phys. Chem.* **1991**, *95*, 7502.
(59) Sottmann, T.; Strey, R.; Chen, S. H. *J. Chem. Phys.* **1997**, *106*, 6483.
(60) Lichterfeld, F.; Schmeling, T.; Strey, R. *J. Phys. Chem.* **1986**, *90*, 5762.
(61) Teubner, M.; Strey, R. *J. Chem. Phys.* **1987**, *87*, 3195.
(62) Chen, S.-H.; Chang, S.-L.; Strey, R. *Prog. Colloid Polym. Sci.* **1990**, *81*, 30.
(63) Porod, G. In *Small Angle X-Ray Scattering*; Glatter, O., Kratky, O., Eds.; Academic: New York, 1982.
(64) Zemb, T. Scattering of Connected Networks. In *Neutron, X-ray and Light Scattering: Introduction to an Investigative Tool for Colloidal and Polymeric Systems*; Lindner, P., Zemb, T., Eds.; Elsevier Science Publications: Amsterdam, The Netherlands, 1991; p 180.
(65) Atkin, R.; Warr, G. G. Bulk and Interfacial Nanostructure in Protic Room Temperature Ionic Liquids. In *Ionic Liquids V: From Knowledge to Application*; Plechkova, N., Seddon, K., Rogers, R., Eds.;in press.
(66) Wakeham, D.; Hayes, R.; Warr, G. G.; Atkin, R. *J. Phys. Chem. B* **2009**, *113*, 5961.

JP910649A